Article

Hydrogen Evolution Reaction Activities of Room-Temperature Self-Grown Glycerol-Assisted Nickel Chloride Nanostructures

Nanasaheb M. Shinde [1,2,*] (ID)**, Siddheshwar D. Raut** [3] (ID)**, Balaji G. Ghule** [4]**, Ramesh J. Deokate** [5] (ID)**,
Sandesh H. Narwade** [4]**, Rajaram S. Mane** [4] (ID)**, Qixun Xia** [6]**, James J. Pak** [1] (ID) **and Jeom-Soo Kim** [2,*]

1   School of Electrical Engineering, Korea University, Seoul 02841, Republic of Korea
2   Department of Chemical Engineering (BK21 FOUR), Dong-A University, 37 Nakdong-daero, Saha-gu,
    Busan 49315, Republic of Korea
3   Department of Future Energy Convergence, Seoul National University of Science & Technology,
    232 Gongneung-ro, Nowon-gu, Seoul 01811, Republic of Korea
4   School of Physical Sciences, Swami Ramanand Teerth Marathwada University, Nanded 431606, India
5   Vidya Pratishtan's Arts, Science and Commerce College, Baramati 413133, India
6   Henan Key Laboratory of Materials on Deep-Earth Engineering, School of Materials Science and Engineering,
    Henan Polytechnic University, Jiaozuo 454000, China
*   Correspondence: nanashinde2009@gmail.com (N.M.S.); jsenergy@dau.ac.kr (J.-S.K.)

Abstract: Three-dimensional nanomaterials of desired structural/morphological properties and highly porous with a high specific surface area are important in a variety of applications. In this work, glycerol-mediated self-growth of 3-D dandelion flower-like nickel chloride ($NiCl_2$) from nickel-foam (NiF) is obtained for the first time using a room-temperature (27 °C) processed wet chemical method for electrocatalysis application. Glycerol-mediated self-grown $NiCl_2$ flowers demonstrate an excellent electrocatalytic performance towards the hydrogen evolution reaction (HER), which is much superior to the NiF (303 mV) and $NiCl_2$ electrode prepared without glycerol (208 mV) in the same electrolyte solution. With a Tafel slope of 41 mV dec^{-1}, the $NiCl_2$ flower electrode confirms improved reaction kinetics as compared to the other two electrodes, i.e., NiF (106 mVdec^{-1}) and $NiCl_2$ obtained without glycerol (56 mV dec^{-1}). The stability of the glycerol-based $NiCl_2$ electrode has further been carried out for 2000 cycles with the overpotential diminution of just 8 mV, approving an electrocatalyst potential of glycerol-based $NiCl_2$ electrode towards HER kinetics. This simple and easy growth process involves nucleation, aggregation, and crystal growth steps for producing $NiCl_2$ nanostructures for electrocatalytic water splitting application through the HER process.

Keywords: self-grown nanostructures; $NiCl_2$; structural elucidation and morphology evolution; electrocatalysis

1. Introduction

The large-scale reliance on fossil fuels, and their predictable reduction, is of serious concern not only for worldwide environmental pollution but also the energy crisis, which has encouraged researchers to look for new renewable and clean energy resources [1–4]. Hydrogen is a viable alternative to fossil fuels [5,6]. After water electrolysis, high-purity hydrogen evolution reactions (HER) take place at the cathode, while the anode produces oxygen evolution reactions (OER). Both HER and OER kinetics are essential for the overall water-splitting process. Because the hydrogen adsorption free energy on these metal surfaces is thermally neutral, platinum group metals are known to be the best HER catalysts [6,7]. Due to the high cost of platinum, its use as an HER catalyst has been substantially limited [8–15]. The development and synthesis of HER catalysts with high catalytic activity are some of the top issues for researchers across the globe. Versatile nickel-based electrodes, including NiS_2, NiO, NiSe, etc., have widely been envisaged for HER as well as OER electrocatalysts [16–22]. An electrocatalyzer assembly consisting of a cathode (platinum–carbon) for the HER with

zero overpotential and an anode (ruthenium oxide/iridium oxide) for the OER with a 1.23 V overpotential for water splitting (at 10 mA cm^{-2} current density) is considered to be a standard measurement [7]. To-date, very few reports describing the use of self-supported Ni-based electrocatalysts in HER studies are known. For example, Zhu et al. revealed an in-situ chemical etching (ICE) approach for obtaining 3D Ni_3S_2 superstructures (needle array and leaf pattern) on a nickel-foam (NF) substrate for probable HER/OER catalyst with the lowest overpotential of 182/340 mV [23]. Shinde et al. have grown promising NiF_2 nanorod arrays directly on a 3D NF via a reduction procedurethat obtained172 mV HER overpotential [24]. According to Wang et al., a NiS/NiF electrode delivered 158 mV overpotential for the HER and 50 mV overpotential for the OER [25]. These processes produce only one form of nanostructure, and their sophisticated customization necessitates the precursor composition ratio variation [26–41]. If the product is in powder form, several annealing courses are required to remove the binders, which eventually can reduce electrochemical performance by obstructing the porosity of the employed matrix or host materials.

This issue has been resolved in this manuscript to some limit by self-growing dandelion flower-like $NiCl_2$@NiF nanostructured electrode material at room-temperature (25°C) in the presence of glycerol. The use of glycerol demonstrates a significant impact on the shape, surface area, and electrochemical performance of 3D $NiCl_2$@NiF nanostructure over pristine NiF and $NiCl_2$@NiF (obtained without glycerol) electrodes. Glycerol in a precursor solution can aid in the formation of a well-controlled dandelion flower-like nanostructure. We present a simple and scalable self-grown wet chemical, i.e., hydrothermal synthesis method, for obtaining the $NiCl_2$@NiF electrode, which is intended for water splitting with a low overpotential of 176 mV for HER electrocatalysis with a Tafel slope of 41 mV dec^{-1} and long-term stability up to 2000 cycles.

2. Results

2.1. Morphology Evolution Studies

The FE-SEM depictions of the $NiCl_2$@NiF electrodes obtained with and without glycerol are shown in Figure 1. From Figure 1a, several nanorods are interlocked with each other and well-cover the 3D NiF skeleton. The diameters of these nanorods are found to be in the range of 1–3 μm, and the average length is 10 (±4) μm. The compact nanorod structure of this electrode may offer a smaller surface area and hence may seriously impact on its electrochemical performance. Moreover, the ion percolation is complicated with the present form of nanorods. So, it is hopefully possible to control the $NiCl_2$ nanostructure using glycerol as a surfactant.

As shown in Figure 1b, well-controlled parallel and conical arranged nanorods are grown together to form dandelion flowers on the NiF (see Figure 1(b-1) for a closer view). Some NiF spaces are exposed, suggesting the selective growth of $NiCl_2$ for obtaining dandelion flower-like architecture from NiF without adding any nickel salt. Compared with Figure 1a, the dandelion flowers are uniformly distributed on the NiF substrate surface, suggestinga decrease in the self-aggregation of $NiCl_2$, which is totally disappeared (Figure 1(b,b-1)). Vertically inclined nanorods are confirmed in the dandelion flowers. These upright standing nanorods have an average height of 10 (±3) μm with a separation distance of 5–10 μm (see Figure 1(b-2)), which will effectively help the deep penetration of the electrolyte ion for majority access and hassle-free charge/mass transportation. Figure S1 shows the related FE-SEM-assisted EDX elemental mapping measurements of the $NiCl_2$ electrodes obtained with and without glycerol (a, a-2 and b, b-2). Both Ni and Cl elements are evenly distributed over the $NiCl_2$ electrode surface (with and without glycerol) in a 1:2 stoichiometric ratio, indicating that the 3D NiF surface has converted to $NiCl_2$. The TEM image of the $NiCl_2$ sample obtained with glycerol, as shown in Figure 1c, clearly displays a dandelion flower-like nanostructure, which is constructed by several nanorods. As screened at higher magnification images, these interconnected nanorods are well-distinguished from one another. The HR-TEM image shown in Figure 1c is a TEM image of the $NiCl_2$ obtained with glycerol where a dandelion flower-like morphology,
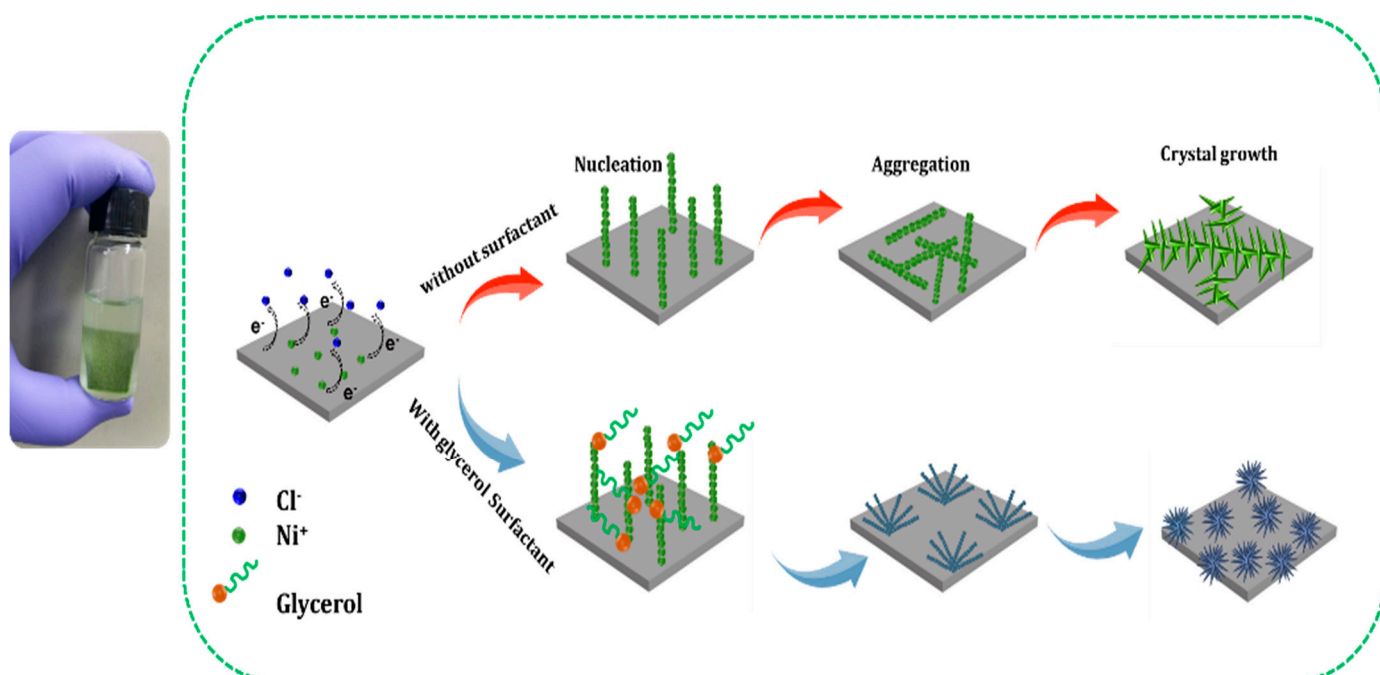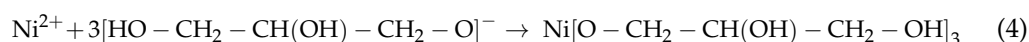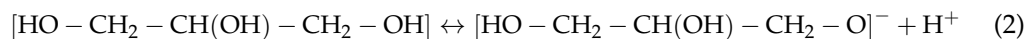
consistent with the FE-SEM image, is constructed by the nanorods, which is consistent with the above FE-SEM observations as shown in the Figure 1b.
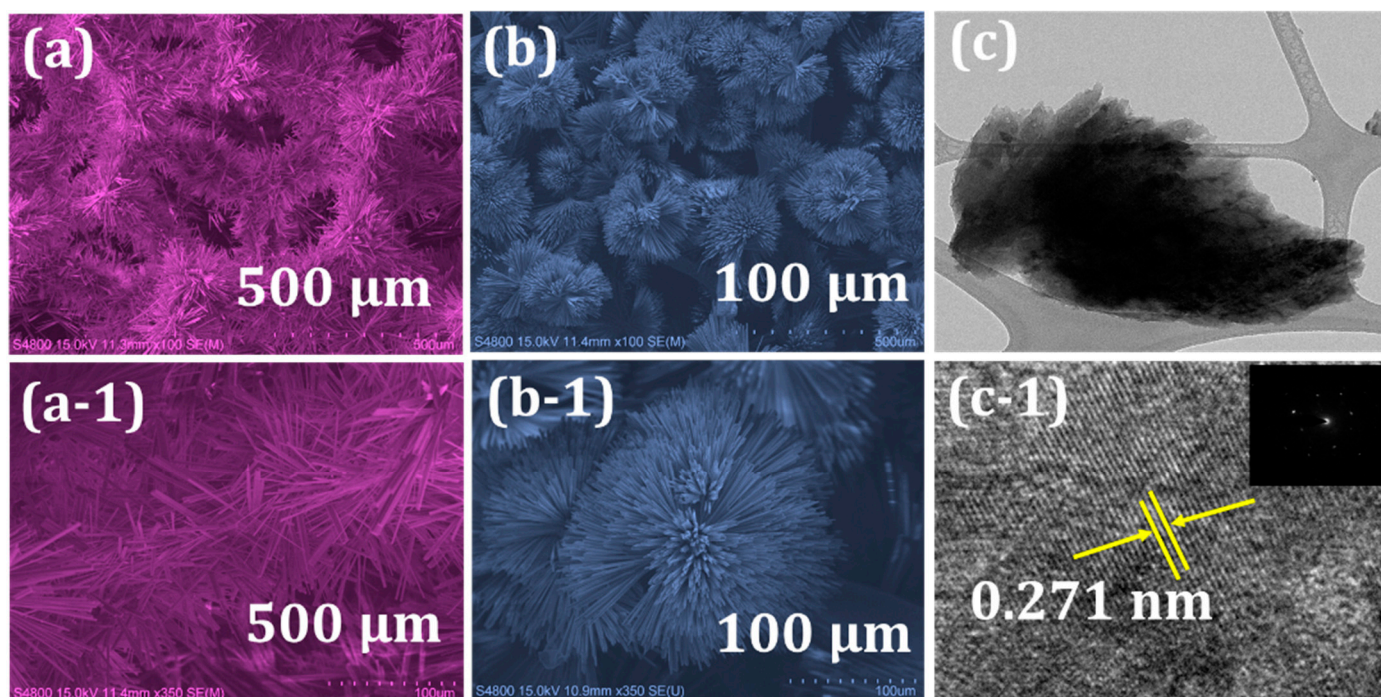
Figure 1. [(**a**,**a-1**,**b**,**b-1**)] False FE-SEM images of $NiCl_2$ obtained with and without glycerol at different magnifications, and (**c**) TEM image; (**c-1**) HR-TEM (inset shows SEAD pattern) of $NiCl_2$ electrode prepared with glycerol.

The formation of the $NiCl_2$ is confirmed by HR-TEM imaging (Figure 1(c,c-1)) as the visible lattice fringes with an interlayer spacing of 0.271 nm, in close agreement with the XRD result (discussed later), are observed. The same part of the nanorods, as seen in the HR-TEM image, does not have clearly reflected lattice fringes, suggesting the presence of an amorphous or non-crystalline$NiCl_2$. The well-ordered circular arrays of lattice points in the selected-area electron diffraction pattern (inset of Figure 1(c-1)) are noted, indicating the significant single crystallinity of the $NiCl_2$ nanorods [32]. The above results suggest that the formation process of the $NiCl_2$ dandelion flowers strongly depends on the use of glycerol in the precursor solution, which has been described as a growth process (see Scheme 1), in which the use of an appropriate amount of glycerol with acetone to form a uniform and transparent mixed solution can act as a micro-emulsion. This can be confirmed to be a Tyndall-effect-free and miscible solvent under thermodynamic equilibrium [40], so it is reasonable to control the self-aggregation of a $NiCl_2$ dandelion flower in precursor solution through the following reaction steps. The NiF is initially oxidized to create nickel ions on the surface when dipped in a homogeneous solution containing acetone, glycerol, and hydrochloric acid (Equation (1)). Glycerol surfactant and hydrochloric acid are disintegrated in acetone at the same time, yielding glycerol, chlorine, and hydrogen free radical ions (see Equations (2) and (3)). Furthermore, Ni^+ ions serve as nucleation sites, attracting glycerol surfactant molecules to create an intermediate complex known as $Ni[O-CH_2-CH(OH)-CH_2-OH]_3$. Furthermore, this intermediate combination transfers electrons to Cl^- ions, converting $NiCl_2$ primary nanorods on the NiF surface, which serves as a basic mother root for the growth of a dandelion flower $NiCl_2$ nanostructure (see bottom reaction pathway of schematic 1). As time proceeds, seed nuclei will grow in the vertical direction without aggregation under the control of the glycerol surfactant (see Scheme 1), forming dandelion flower-type $NiCl_2$, which is summarized in flowing reaction kinetics [32]. On the other hand, in the case of the $NiCl_2$ sample prepared without glycerol surfactant, the growth of the $NiCl_2$ nanorods is out of control; hence the formation of

scattered and irregular nanorods over the NiF surface (see upper reaction pathway in Scheme 1) is seen. A very similar type of growth mechanism for the Fe_2O_3 nanoparticles obtained in the presence of glycerol has been reported elsewhere [32,40].

$$Ni - foam \rightarrow Ni^{2+} \tag{1}$$

$$[HO - CH_2 - CH(OH) - CH_2 - OH] \leftrightarrow [HO - CH_2 - CH(OH) - CH_2 - O]^- + H^+ \tag{2}$$

$$HCl \rightarrow H^+ + Cl^- \tag{3}$$

$$Ni^{2+} + 3[HO - CH_2 - CH(OH) - CH_2 - O]^- \rightarrow Ni[O - CH_2 - CH(OH) - CH_2 - OH]_3 \tag{4}$$

$$Ni[O - CH_2 - CH(OH) - CH_2 - OH]_3 + 2Cl^- \rightarrow NiCl_2 \tag{5}$$

Scheme 1. Self-growth of $NiCl_2$@NiF nanostructures with and without glycerol surfactant.

2.2. Structural Elucidation

Figure 2 confirms the X-ray diffraction patterns of the $NiCl_2$ electrode materials on the NiF obtained with and without glycerol (A and B). Two intensive peaks, marked as symbol '∆', of metallic nickel (see Figure 2a(C)) in all patterns are recognized ((JCPDS card no. 04-0850)). The newly reflected diffraction peaks denoted with a '*' symbol and positioned at a different 2-theta location according to JCPDS card no. 01-072-0044 are assigned to $NiCl_2$. According to the XRD results, the intensity of the diffraction peak in the glycerol-meditated $NiCl_2$ sample is higher compared to the non-glycerol-involved sample, showing higher crystallinity in the prior over the latter. The detailed surface optimization of the glycerol-mediated $NiCl_2$ electrode was obtained using XPS, and the corresponding results are presented in Figure 2b–d. The presence of Ni and Cl elements is confirmed by the survey spectrum (Figure 2b). The deconvoluted Ni 2p high-resolution spectrum (Figure 2c) adduces two major peaks at 856.3 and 874.1 eV for Ni $2p_{3/2}$ and Ni $2P_{1/2}$, respectively, with a spin energy separation distance of 17.8 eV. The satellite peaks at 862.2 and 882.5 eV, which are in good agreement with previous findings, are also evidenced [32].
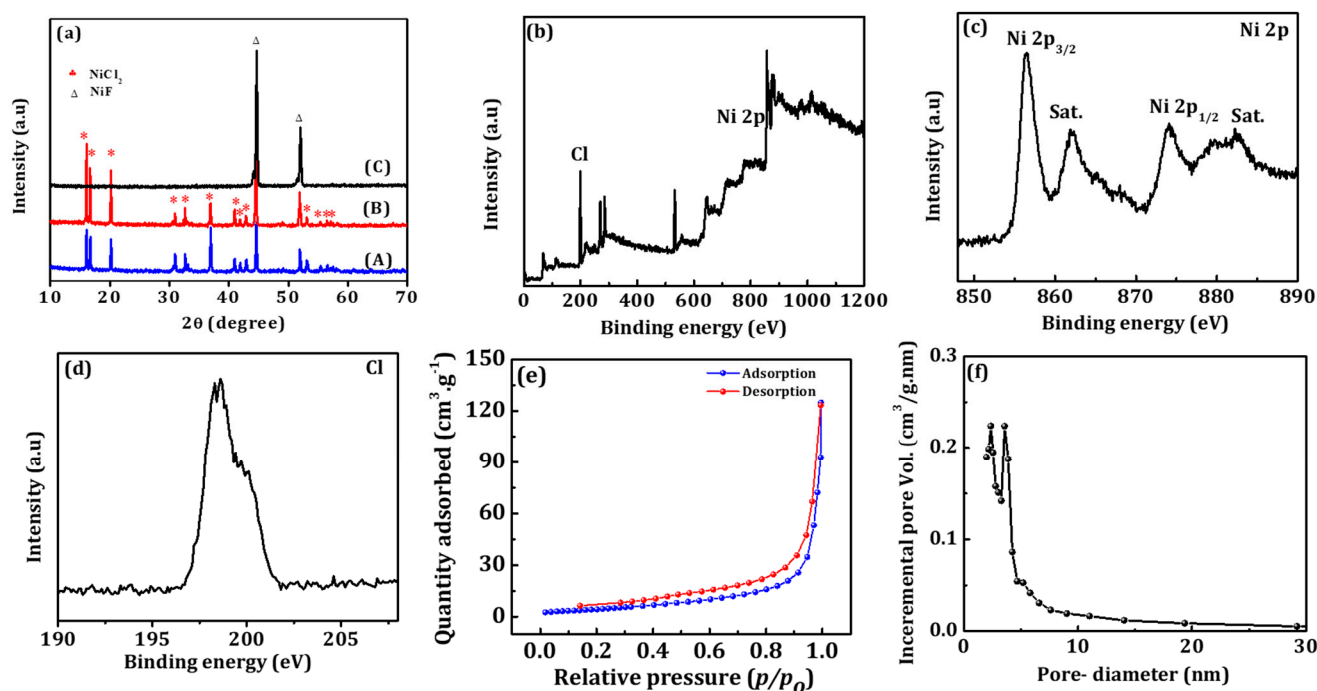
Figure 2. (**a**) XRD patterns (A and B) electrode with and without glycerol $NiCl_2$ and C (i.e., NiF), (**b**) full XPS spectrum survey, (**c**) Ni 2p, (**d**) Cl, (**e**) BET and (**f**) pore size distribution of electrode with glycerol, respectively.

The prominent peak obtained at 198.56 eV in the Cl high-resolution spectrum indicates that $NiCl_2$ develops on the NiF skeleton during the self-growth process at ambient temperature. The specific surface area (IV-type isotherm and H_3 hysteresis type), pore-size distribution, and pore surface area estimations of the optimized with glycerol-mediated $NiCl_2$ electrode determined by N_2 adsorption–desorption measurements are, respectively, 15.98 m^2g^{-1}, 7.4 nm, and 47.66 m^2g^{-1} (Figure 2e) [32]. The nature of the adsorption and the desorption branches is assigned to the mesoporous behavior [32].

2.3. HER Activity

Furthermore, $NiCl_2$ electrocatalysts i.e., prepared with and without glycerol were utilized to study the HER water catalysis activity in 1.0 M KOH electrolyte solution (Figure 3) and compared with pristine NiF.

The polarization curves of the as-prepared with and without glycerol-mediated $NiCl_2$ electrode materials are shown in Figure 3a. Both electrode materials demonstrate considerable HER activity. As compared to the nanorod-type $NiCl_2$ (208 mV and pristine NiF (303 mV) electrodes, the 'with dandelion flower-like $NiCl_2$ electrode reveals an enhanced electrocatalytic activity with as small as 176 mV overpotential, proving an enhancement in electrocatalytic activity due to the change in morphology caused by the glycerol incorporation of the $NiCl_2$ electrode for HER. The Tafel slopes for the corresponding electrode materials, as shown in Figure 3b, are lowered from 41 mV dec^{-1} to 57 mV dec^{-1} when the HER rate is increased (see supporting information (SI) for more details on the equations used for computation). The Volmer–Heyrovsky mechanism is obeyed on the electrode surface, as evidenced by the tiny Tafel slope of 41 $mVdec^{-1}$ [39–42]. As shown in Figure 3c, the electrochemical impedance spectroscopy (EIS) analysis performed for the three aforementioned electrodes from the 100 kHz to 10 kHz frequency range with a potential amplitude of 5 mV adduces clear and visible difference. Compared to the $NiCl_2$ obtained without glycerol and pristine NiF electrodes, the glycerol-mediated $NiCl_2$ electrode has low equivalent series resistance (2.62 Ω) and 1.78 Ω charge transfer resistance, the $NiCl_2$ electrode obtained with glycerol has improved electron mobility and electrocatalytic

activity [24,41]. The cyclability test of the dandelion flower-type $NiCl_2$ electrocatalyst for HER was further examined by successive CV plots in a three-electrode system at a scan rate of 10 mV s^{-1} for 2000 cycles (Figure 3d). A negligible decrease of 8 mV has been noticed in the 1st and 2000th polarization curves after long-term HER activity scanning, demonstrating its excellent HER catalytic ability with moderate chemical stability. The inset of Figure 3d presents a genuine photograph of the three-electrode system used for the electrocatalytic study, where a clear progression of oxygen bubble evaluation, indicating strong HER activity, is confirmed. This obtained over-potential is comparable with those reported in the literature (Table 1). According to the electrocatalysis results, the glycerol-containing $NiCl_2$ electrode exhibits excellent catalytic activity and stability towards the HER for several reasons (Scheme 2), which are as follows; (i) the porous nano-array structure of dandelion flower with a high surface area results in a greater number of active sites for electrocatalytic activity, (ii) the direct binder-free growth of mesoporous dandelion flower-like $NiCl_2$ on 3D conductive NiF substrate provides good connectivity with zero dead volume, (iii) the direct deposition of the $NiCl_2$ dandelion flower on the NiF surface and the close interconnection of these nanorods, forming a network that maintains good structural stability with efficient electron transport, and (iv) the room-temperature $NiCl_2$ synthesis approach as shown in Scheme 2 clearly depicts the important features of the dandelion flower-type structure for better catalytic performance.
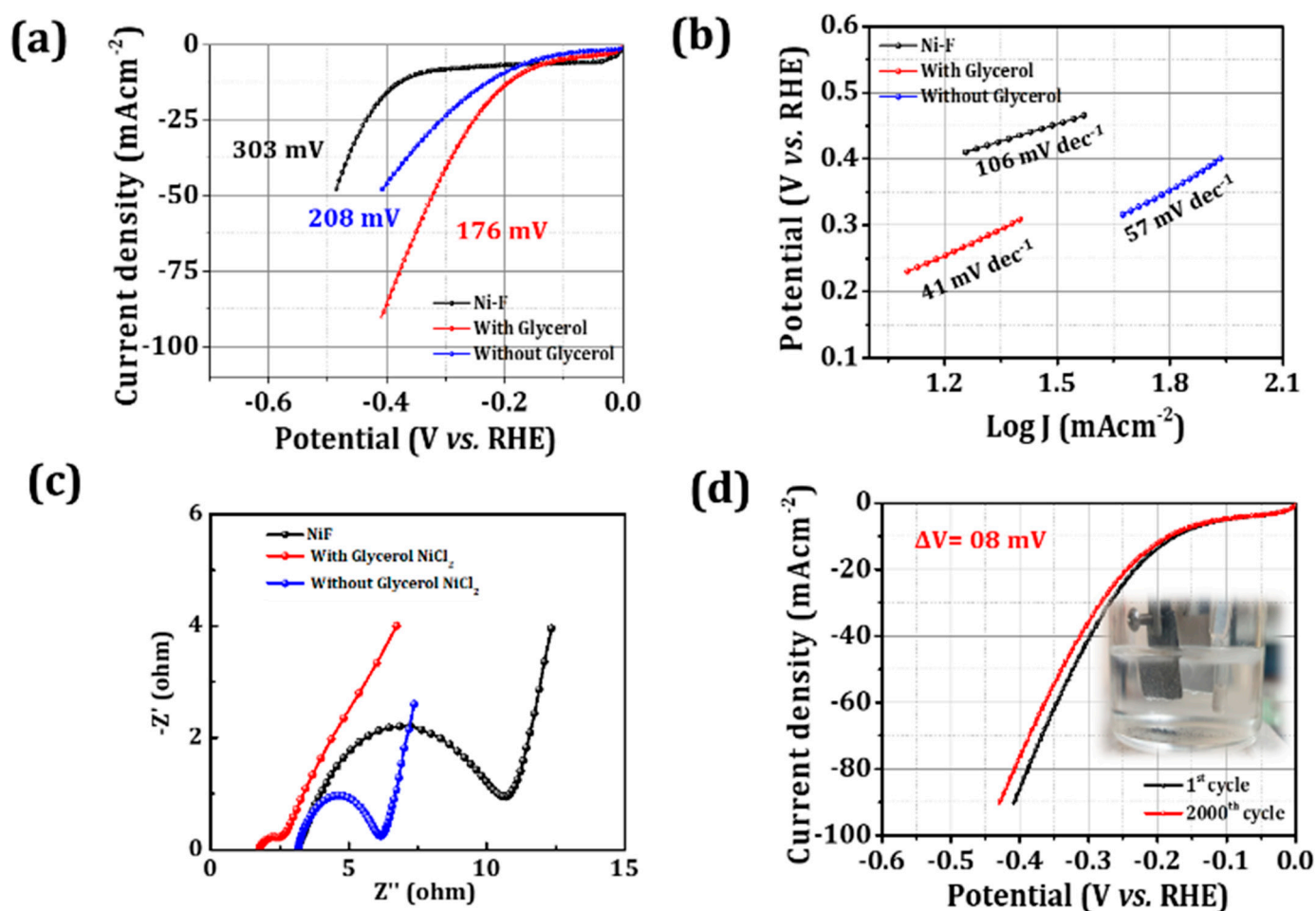
Figure 3. (**a**) HER polarization curves, (**b**) Tafel plots, and (**c**) EIS spectroscopy measurements of NiF and $NiCl_2$ (with and without glycerol) electrode materials. (**d**) Cyclic stability test (inset shows the real-time image of H_2 evolution reaction) of dandelion flower-type $NiCl_2$.

Table 1. The comparative set up showing HER activities of present work with reported data.

Catalysts	Electrolyte	η (mV)	Tafel Slope (mV dec^{-1})	J (mA cm^{-2})	Ref.
Ni$_2$P@NSG	1.0 M KOH	110	43	10	[42]
NiFeCo	1.0 M KOH	108	64	10	[43]
NiS/Ni$_2$P/carbon cloth	1.0 M KOH	111	78.1	20	[44]
NiS/NiS$_2$	1.0 M KOH	248	142.3	10	[45]
Fe- NiS$_2$	0.5 M H$_2$SO$_4$	198	42	10	[46]
NiS$_2$	1.0 M KOH	219	157	10	[47]
NiS$_2$/graphite substrate	0.5 M H$_2$SO$_4$	240	41	10	[48]
Te@NiTe$_2$/NiS/acetylene black	1.0 M KOH	101	118	10	[49]
NiTe$_2$	0.5 M H$_2$SO$_4$	560	44	10	[50]
Ni$_3$Te$_2$	1.0 M KOH	304	94.2	10	[51]
NiSSe	1.0 M KOH	154	125	10	[52]
NiF	0.5 M H$_2$SO$_4$	210	1006.6	10	[53]
NiF$_2$	0.1 M KOH	172	47	10	[12]
NiCl$_2$	1.0 M KOH	176	41	10	Current work
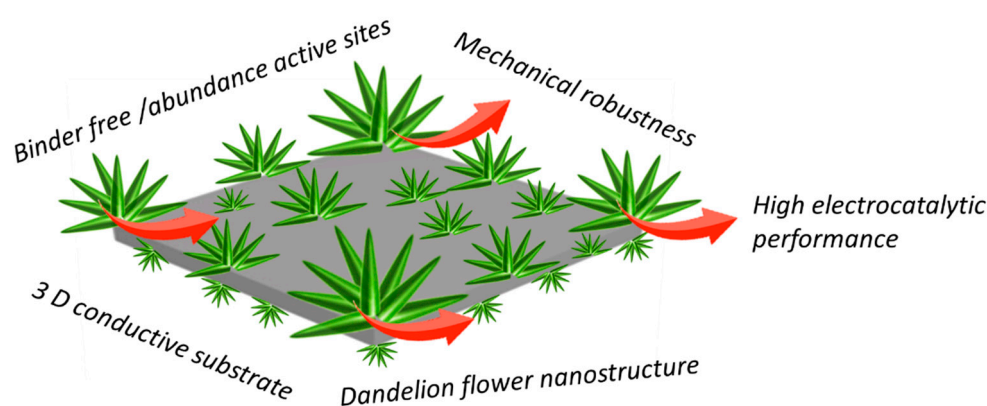
Scheme 2. Schematic presentation showing various causes responsible for the enhanced catalytic performance of dandelion flower-type NiCl$_2$ catalyst towards the HER.

3. Materials and Methods

3.1. Chemicals

NiF, with a pore density of 110 pore size and a mass density of 320 g m^{-2}, was obtained (Artenano Company Limited, Central, Hong Kong). Concentrated hydrochloric acid (HCl, 37%) was obtained from Daejung Chemicals (Seongnam-si, Republic of Korea). Acetone and anhydrous ethanol standard solutions were purchased from SK Chemicals (Seongnam-si, Republic of Korea). Deionized (DI) water, obtained from (Millipore Darmstadt, Darmstadt, Germany), was used throughout the experiments as a solvent. The NiCl$_2$ dandelion flowers were fabricated under optimized conditions on NiF at room-temperature. A NiF (2.00 × 6.00 cm^2) was ultrasonicated for 20 minin ethanol, acetone, and finally, water to ensure that the NiF surface was thoroughly cleaned and then dried in a vacuum oven at 60 °C for 12 h using a process described elsewhere [32]. The NiF was then placed in a glass falcon tube (25 mL) that was filled with 20 mL acetone and 0.1 M HCl, in addition to a few drops of glycerol, which was stirred continuously for 10 min. The glass falcon tube was then sealed with a lid and left at room-temperature for 4 h. Interestingly, after a few hours, the NiF was changed from a polished silvery texture to a rough texture with a bright green tint (see on-ground experimental digital images displayed in Scheme 1). Finally, the NiF was removed and properly washed with deionized water multiple times before being thoroughly dried in a vacuum at 60 °C for 12 h and labeled as electrode 'with glycerol'. For comparison, a NiCl$_2$

sample was obtained under identical conditions but just without the addition of glycerol into the for mentioned solution, which was referred to as 'without glycerol'.

3.2. Characterizations

The structural interpretation and surface morphology evolution studies for the $NiCl_2$ electrodes, i.e., with and without glycerol, were carried out using X-ray diffraction (XRD, D8-Discovery Bruker, 40 kV, 40 mA, Cu Kα, λ = 1.5406 Å) patterns and field-emission scanning electron microscopy (FE-SEM, Hitachi, S-4800, 15 kV) digital images, equipped with an energy-dispersive X-ray spectroscopy (EDX) measurement unit. Both transmission and high-resolution transmission electron microscopy (HRTEM, JEOL 2100F) images were recorded over the optimized $NiCl_2$ nanostructured electrode. The X-ray photoelectron spectroscopy (XPS, VG Scientifics ESCALAB250) measurement was carried out to analyze the chemical bonding status of the $NiCl_2$ nanostructures. The surface area and pore-size distribution for the $NiCl_2$ nanostructures were obtained from Brunauer–Emmett–Teller (BET) and Barrett–Joyner–Halenda (BJH) plots.

3.3. HER Confirmation

Both $NiCl_2$ nanostructure electrocatalysts were envisaged in a three-electrode system (in addition to NiF as a reference) in the presence of a Hg/HgO reference electrode and a platinum counter electrode. A nitrogen purge was used for 10 min before the trials to normalize the system in terms of external and internal oxygen.

3.4. Formulae Used

The formulae used for estimating the overpotential and the Tafel slope are provided in the supporting information.

4. Conclusions

In summary, the glycerol-mediated self-growth of dandelion flower-type $NiCl_2$ nanostructure is proposed at room-temperature viaa soft chemical approach. After sorting out the phase formation confirmation through the XRD pattern analysis. Change in the dandelion flower-type surface appearance with the 15.98 m^2g^{-1} surface area of the as-obtained $NiCl_2$ on glycerol loading has been evidenced by the FE-SEM images and BJH curves, respectively. Furthermore, the HER activities of the aforementioned electrodes studied for water-splitting applications demonstrate the feasibility of $NiCl_2$ as an HER electrode material in the water-splitting process. The $NiCl_2$ electrode prepared in the presence of glycerol demonstrates an overpotential of 176 mV, while the electrode prepared without glycerol confirms the overpotential of 208 mV, suggesting the impact of surface modification on HER performance. The $NiCl_2$ dandelion flower-like electrode reveals the superior reaction kinetics with the small Tafel slope of 41 mV dec^{-1} as compared to that of the nanorod-type $NiCl_2$ (57 mV dec^{-1}) electrode obtained without glycerol. Moreover, the $NiCl_2$ dandelion flower electrode is found to be stable even after 2000 operation cycles with a minute decrease of 8 mV in overpotential. The considerable HER activity of the $NiCl_2$ dandelion flower-type electrode is attributed to its high surface area, flower-like morphology, and low internal resistance due to uncomplicated charge transport.

Author Contributions: Conceptualization, N.M.S., B.G.G., N.M.S. and S.D.R.; methodology, N.M.S. and S.H.N.; software, R.J.D.; validation, N.M.S., B.G.G. and Q.X.; formal analysis, N.M.S. and Q.X.; investigation, N.M.S. and S.D.R.; data curation, N.M.S.; writing—original draft preparation, R.S.M., J.-S.K., J.J.P.; review and editing, visualization, supervision, R.S.M., J.-S.K., J.J.P. All authors have read and agreed to the published version of the manuscript.

Data Availability Statement: Not applicable.

Conflicts of Interest: The authors declare no conflict of interest.

References

1. Zhou, G.; Wang, P.; Li, H.; Hu, B.; Sun, Y.; Huang, R.; Liu, L. Spin-state reconfiguration induced by alternating magnetic field for efficient oxygen evolution reaction. *Nat. Commun.* **2021**, *12*, 4827. [CrossRef]
2. Anantharaj, S.; Rao Ede, S.; Sakthikumar, K.; Karthick, K.; Mishra, S.; Kundu, S. A Recent Trends and Perspectives in Electrochemical Water Splitting with an Emphasis on Sulfide, Selenide, and Phosphide Catalysts of Fe, Co, and Ni: A Review. *ACS Catal.* **2016**, *6*, 8069–8097. [CrossRef]
3. Zhou, G.; Wang, P.; Hu, B.; Shen, X.; Liu, C.; Tao, W.; Huang, P.; Liu, L. Spin-related symmetry breaking induced by half-disordered hybridization in BixEr$_2$-xRu$_2$O$_7$ pyrochlores for acidic oxygen evolution. *Nat. Commun.* **2022**, *13*, 4106. [CrossRef]
4. Suen, N.; Hung, S.; Quan, Q.; Zhang, N.; Xu, Y.; Chen, M. Electrocatalysis for the Oxygen Evolution Reaction: Recent Development and Future Perspectives. *Chem. Soc. Rev.* **2017**, *46*, 337–365. [CrossRef]
5. Zhou, G.; Shan, Y.; Wang, L.; Hu, Y.; Guo, J.; Hu, F.; Shen, J.; Gu, Y.; Cui, J.; Liu, L.; et al. Photoinduced semiconductor-metal transition in ultrathin troilite FeS nanosheets to trigger efficient hydrogen evolution. *Nat. Commun.* **2019**, *10*, 399. [CrossRef]
6. Fu, Y.; Shan, Y.; Zhou, G.; Long, L.; Wang, L.; Yin, K.; Guo, J.; Shen, J.; Liu, L.; Wu, X. Electric strain in dual metal Janus nanosheets induces structural phase transition for efficient hydrogen evolution. *Joule* **2019**, *3*, 2955–2967. [CrossRef]
7. Chaudhari, N.; Jin, H.; Kim, B.; Lee, K. Nanostructured Materials on 3D Nickel Foam as Electrocatalysts for Water Splitting. *Nanoscale* **2017**, *9*, 12231–12247. [CrossRef]
8. Giri, A.; Park, G.; Yang, H.; Pal, M.; Kwak, J.; Jeong, U. Synthesis of 2D Metal Chalcogenide Thin Films through the Process Involving Solution-Phase Deposition. *Adv. Mater.* **2013**, *30*, 1707577. [CrossRef]
9. Chou, S.; Lin, J. Cathodic Deposition of Flaky Nickel Sulfide Nanostructure as an Electroactive Material for High-Performance Supercapacitors. *J. Electrochem. Soc.* **2013**, *160*, D178–D182. [CrossRef]
10. Yu, S.; Yoshimura, M. Ferrite/Metal Composites Fabricated by Soft SolutionProcessing. *Adv. Funct. Mater.* **2002**, *12*, 277–285. [CrossRef]
11. Yang, S.; Yao, H.; Gao, M.; Yu, S. Monodisperse Cubic Pyrite NiS$_2$ Dodecahedrons and Microspheres Synthesized by a Solvothermal Process in a Mixed Solvent: Thermal Stability and Magnetic Properties. *CrystEngComm* **2009**, *11*, 1383–1390. [CrossRef]
12. Li, X.; Li, Q.; Wu, Y.; Rui, M.; Zeng, H. Two-Dimensional, Porous Nickel–Cobalt Sulfide for High-Performance Asymmetric Supercapacitors. *ACS Appl. Mater. Interf.* **2015**, *7*, 19316–19323. [CrossRef] [PubMed]
13. Yang, Q.; Lu, Z.; Liu, J.; Lei, X.; Chang, Z.; Luo, L.; Sun, X. Metal oxide and Hydroxide Nanoarrays: Hydrothermal Synthesis and Applications as Supercapacitors and Nanocatalysts. *Prog. Nat. Sci. Mater. Int.* **2013**, *23*, 351–366. [CrossRef]
14. Liu, Y.; Li, Y.; Kang, H.; Jin, T.; Jiao, L. Design, Synthesis, and Energy-related Applications of Metal Sulfides. *Mater. Horiz.* **2016**, *3*, 402–421. [CrossRef]
15. Guo, K.; Yang, F.; Cui, S.; Chen, W.; Mi, L. Controlled synthesis of 3D Hierarchical NiSe Microspheres for High-performance Supercapacitor Design. *RSC Adv.* **2016**, *6*, 46523–46530. [CrossRef]
16. Lin, H.; Liu, F.; Wang, X.; Ai, Y.; Yao, Z.; Chu, L.; Han, S.; Zhuang, X. Graphene-Coupled Flower-Like Ni3S2 for a Free-Standing 3D Aerogel with an Ultra-High Electrochemical Capacity. *Electrochim. Acta* **2016**, *191*, 705–715. [CrossRef]
17. Zhang, Y.; Qian, L.; Zhao, W.; Li, X.; Huang, X.; Mai, X.; Wang, Z.; Shao, Q.; Yan, X.; Guo, Z. Highly Efficient Fe-N-C Nanoparticles Modified Porous Graphene Composites for Oxygen Reduction Reaction. *J. Electrochem. Soc.* **2018**, *165*, H510–H516. [CrossRef]
18. Krishnamoorthy, K.; Kumar Veerasubramani, G.; Radhakrishnan, S.; Kim, S. One pot Hydrothermal Growth of Hierarchical Nanostructured Ni$_3$S$_2$ on Ni foamfor Supercapacitor Application. *Chem. Eng. J. Chem.* **2014**, *251*, 116–122.
19. Zhuo, M.; Zhang, P.; Chen, Y.; Li, Q. Facile Construction of Graphene-likeNi$_3$S$_2$ Nanosheets Through the Hydrothermally Assisted Sulfurization of NickelFoam and Their Application as Self-supported Electrodes for Supercapacitors. *RSC Adv.* **2015**, *5*, 25446–25449. [CrossRef]
20. Li, W.; Wang, S.; Xin, L.; Wu, M.; Lou, X. Single-crystal β-NiS Nanorod Arrays with a Hollow-structured Ni$_3$S$_2$ Framework for Supercapacitor Applications. *J. Mater. Chem. A* **2016**, *4*, 7700–7709. [CrossRef]
21. Li, J.; Wang, S.; Xiao, T.; Tana, X.; Xiang, P.; Jiang, L.; Deng, C.; Li, W.; Li, M. Controllable preparation of Nanoporous Ni$_3$S$_2$ films by Sulfuration of nickel foam as promising asymmetric supercapacitor electrodes. *Appl. Surf. Sci.* **2017**, *420*, 919–926. [CrossRef]
22. Zhang, D.; Li, J.; Luo, J.; Xu, P.; Wei, L.; Zhou, D.; Xu, W.; Yuan, D. Ni$_3$S$_2$ nanowires grown on nickel foam as an efficient bifunctional electrocatalyst for water splitting with greatly practical prospects. *Nanotechnology* **2018**, *29*, 245402. [CrossRef] [PubMed]
23. Zhu, T.; Zhu, L.; Wang, J.; Ghim, H. In Situ Chemical Etching of Tunable 3D Ni$_3$S$_2$ Superstructures For Bifunctional Electrocatalysts For Overall Water Splitting. *J. Mater. Chem. A* **2016**, *4*, 13916–13922. [CrossRef]

24. Shinde, N.; Raut, S.; Ghule, B.; Gunturu, K.; Pak, J.; Mane, R. Recasting Ni-foam into NiF$_2$ nanorod arrays via a hydrothermal process for hydrogen evolution reaction application. *Dalton Trans.* **2021**, *50*, 6500–6505. [CrossRef] [PubMed]

25. Zhu, W.; Yue, X.; Zhang, W.; Yu, S.; Zhang, Y.; Wang, J.; Wang, J. Nickel sulfide Microsphere Film on Ni foam as an Efficient Bifunctional Electrocatalyst for Overall Water Splitting. *J. Chem. Commun.* **2016**, *52*, 1486–1489. [CrossRef] [PubMed]

26. Maiaugree, W.; Tangtrakarn, A.; Lowpa, S.; Ratchapolthavisin, N.; Amornkitbamrung, V. Facile Synthesis of Bilayer Carbon/Ni$_3$S$_2$Nanowalls for a Counter Electrode of Dye-sensitized Solar Cell. *Electrochim. Acta* **2015**, *174*, 955–962. [CrossRef]

27. Li, X.; Chen, Y.; Zou, J.; Zeng, X.; Zhou, L.; Huang, H. Stable Freestanding Li-ion Battery Cathodes by in Situ Conformal Coating of Conducting PolypyrroleonNiS-carbon Nanofiber Films. *J. Power Sources* **2016**, *331*, 360–365. [CrossRef]

28. Salavati-niasari, M.; Davar, F.; Emadi, H. Hierarchical Nanostructured Nickel sulfide architectures through Simple Hydrothermal Method in the Presence of Thioglycoloic Acid. *Chalco. Lett.* **2010**, *7*, 647–655.

29. Al-Naggar, H.; Shinde, N.M.; Kim, J.; Mane, R.S. Water splitting performance of metal and non-metal-doped transition metal oxide electrocatalysts. *Coord. Chem. Rev.* **2022**, *474*, 21486–21644.

30. Feng, N.; Hu, D.; Wang, P.; Sun, X.; Li, X.; He, D. Growth of Nanostructured Nickel Sulfide Films on Ni foam as High-performance Cathodes for Lithium ion Batteries. *Phys. Chem. Chem. Phys.* **2013**, *15*, 9924–9930. [CrossRef]

31. Liang, K.; Marcus, K.; Guo, L.; Li, Z.; Zhou, L.; Li, Y.; De Oliveira, S.; Orlovskaya, N.; Sohn, Y.; Yang, Y. A freestanding NiS$_x$ Porous Film as a Binder-free Electrode for Mg-ion Batteries. *Chem. Commun.* **2017**, *53*, 7608–7611. [CrossRef] [PubMed]

32. Shinde, N.M.; Shinde, P.V.; Yun, J.M.; Mane, R.S.; Kim, K.H. Room-temperature chemical synthesis of 3-D dandelion-type nickel chloride (NiCl$_2$@ NiF) supercapattery nanostructured materials. *J. Colloid Interface Sci.* **2020**, *578*, 547–554. [CrossRef] [PubMed]

33. Yan, S.; Shi, Y.; Sun, L.; Xiao, Z.; Sun, B.; Xu, X. Controlled Synthesis of NiSNanoparticle/CdS Nanowire Heterostructures via Solution Route and Their Optical Properties. *Mater. Sci. Eng. B* **2013**, *178*, 109–116. [CrossRef]

34. Cheng, Z.; Abernathy, H.; Liu, M. Raman Spectroscopy of Nickel SulfideNi$_3$S$_2$. *J. Phys. Chem. C* **2007**, *111*, 17997–18000. [CrossRef]

35. Akbarzadeh, R.; Dehghani, H.; Behnoudnia, F. Sodium Thiosulfate-assisted Synthesis of NiS$_2$ Nanostructure by Using Nickel (II)-Salen Precursor: Optical and Magnetic Properties. *Dalton Trans.* **2014**, *43*, 16745–16753. [CrossRef]

36. Dong, J.; Cheng, Z.; Zha, S.; Liu, M. Identification of Nickel Sulfides on Ni-YSZ Cermet Exposed to H$_2$ Fuel Containing H$_2$S Using Raman spectroscopy. *J. Power Sources* **2006**, *156*, 461–465. [CrossRef]

37. Li, H.; Chai, L.; Wang, X.; Wu, X.; Xi, G.; Liu, Y.; Qian, Y. Hydrothermal Growth and Morphology Modification of β-NiS Three-Dimensional Flowerlike Architectures. *Cryst. Growth Des.* **2007**, *7*, 1919–1920. [CrossRef]

38. Lin, T.; Shuan, C.; Hung, K. High Energy Density Asymmetric supercapacitor Based on NiOOH/Ni$_3$S$_2$/3D Graphene and Fe$_3$O$_4$/Graphene Composite Electrodes. *Sci. Rep.* **2014**, *4*, 7274. [CrossRef]

39. Jing, F.; Lv, Q.; Xiao, J.; Wang, Q.; Wang, S. Highly Active and Dual-function Self-Supported Multiphase NiS–NiS$_2$–Ni$_3$S$_2$/NF Electrodes for Overall Water Splitting. *J. Mater. Chem. A* **2018**, *6*, 14207–14214. [CrossRef]

40. Kang, D.; Hu, C.; Zhu, Q. Morphology controlled synthesis of hierarchical structured Fe$_2$O$_3$ from natural ilmenite and its high performance for dyes adsorption. *App. Sur. Sci.* **2018**, *459*, 327–335. [CrossRef]

41. Deng, J.; Ren, P.; Deng, D.; Yu, L.; Yang, F.; Bao, X. Highly active and durable non-precious-metal catalysts encapsulated in carbon nanotubes for hydrogen evolution reaction. *Energy Environ. Sci.* **2014**, *7*, 1919–1923. [CrossRef]

42. Suryawanshi, U.P.; Ghorpade, U.V.; Lee, D.M.; He, M.; Shin, S.W.; Kumar, P.V.; Jang, J.S.; Jung, H.R.; Suryawanshi, M.P.; Kim, J.H. Colloidal Ni2P Nanocrystals Encapsulated in Heteroatom-Doped Graphene Nanosheets: A Synergy of 0D@ 2D Heterostructure Toward Overall Water Splitting. *Chem. Mater.* **2020**, *33*, 234–245. [CrossRef]

43. Babar, P.; Lokhande, A.; Karade, V.; Pawar, B.; Gang, M.G.; Pawar, S.; Kim, J.H. Bifunctional 2D electrocatalysts of transition metal hydroxide nanosheet arrays for water splitting and urea electrolysis. *ACS Sustain. Chem. Eng.* **2019**, *7*, 10035–10043. [CrossRef]

44. Xiao, X.; Huang, D.; Fu, Y.; Wen, M.; Jiang, X.; Lv, X.; Li, M.; Gao, L.; Liu, S.; Wang, M.; et al. Engineering NiS/Ni$_2$P heterostructures for efficient electrocatalytic water splitting. *ACS Appl. Mater. Interfaces* **2018**, *10*, 4689–4696. [CrossRef]

45. Li, Q.; Wang, D.; Han, C.; Ma, X.; Lu, Q.; Xing, Z.; Yang, X. Construction of amorphous interface in an interwoven NiS/NiS$_2$ structure for enhanced overall water splitting. *J. Mater. Chem. A* **2018**, *6*, 8233–8237. [CrossRef]

46. Wang, T.; Guo, X.; Zhang, J.; Xiao, W.; Xi, P.; Peng, S.; Gao, D. Electronic structure modulation of NiS$_2$ by transition metal doping for accelerating the hydrogen evolution reaction. *J. Mater. Chem. A* **2019**, *7*, 4971–4976. [CrossRef]

47. Tian, T.; Huang, L.; Ai, L.; Jiang, J. Surface anion-rich NiS$_2$ hollow microspheres derived from metal–organic frameworks as a robust electrocatalyst for the hydrogen evolution reaction. *J. Mater. Chem. A* **2017**, *5*, 20985–20992. [CrossRef]

48. Wu, X.; Yang, B.; Li, Z.; Lei, L.; Zhang, X. Synthesis of supported vertical NiS$_2$ nanosheets for hydrogen evolution reaction in acidic and alkaline solution. *RSC Adv.* **2015**, *5*, 32976–32982. [CrossRef]

49. Fan, M.; Li, X.; Wei, D.; Wang, Y.; Li, M. Fabrication of Te@ NiTe$_2$/NiS heterostructures for electrocatalytic hydrogen evolution reaction. *Electrochim. Acta* **2019**, *328*, 135075.

50. Chia, X.; Sofer, Z.; Luxa, J.; Pumera, M. Unconventionally layered CoTe$_2$ and NiTe$_2$ as electrocatalysts for hydrogen evolution. *Chem. A Eur. J.* **2017**, *23*, 11719–11726. [CrossRef]

51. De Silva, U.; Masud, J.; Zhang, N.; Hong, Y.; Liyanage, W.P.; Zaeem, M.A.; Nath, M. Nickel telluride as a bifunctional electrocatalyst for efficient water splitting in alkaline medium. *J. Mater. Chem. A* **2018**, *6*, 7608–7622. [CrossRef]

52. Al-Enizi, A.M.; Shaikh, S.F.; Ubaidullah, M.; Ghanem, M.A.; Mane, R.S. Self-grown one-dimensional nickel sulfo-selenide nanostructured electrocatalysts for water splitting reactions. *Int. J. Hydrog. Energy* **2020**, *45*, 15904–15914. [CrossRef]
53. Lu, J.; Xiong, T.; Zhou, W.; Yang, L.; Tang, Z.; Chen, S. Metal nickel foam as an efficient and stable electrode for hydrogen evolution reaction in acidic electrolyte under reasonable overpotentials. *ACS Appl. Mater. Interfaces* **2016**, *8*, 5065–5069. [CrossRef] [PubMed]